International Journal of Nanoelectronics and Materials
IJNeaM
ISSN 1985-5761 | E-ISSN 2232-1535

Synergistic effect of manganese co-doping on densification, mechanical integrity and ionic conductivity of samarium-doped ceria electrolytes for intermediate-temperature solid oxide fuel cell applications

Edward Cheong Chee Yu [a], Salmie Suhana Che Abdullah [a,b]*, Zuradzman Mohamad Razlan [c], Imaduddin Helmi Wan Nordin [c], Rohaya Abdul Malek [a,b], Abul K Azad [d], and Nur Hidayah Ahmad Zaidi [a,b]

[a]*Faculty of Chemical Engineering & Technology, Universiti Malaysia Perlis (UniMAP), 02600 Arau, Perlis, Malaysia*
[b]*Centre of Excellence for Frontier Materials Research (CFMR), Universiti Malaysia Perlis (UniMAP), Jalan Kangar - Alor Setar, 01000 Kangar, Perlis, Malaysia.*
[c]*Faculty of Mechanical Engineering & Technology, Universiti Malaysia Perlis (UniMAP), Kampus Tetap Pauh Putra, 02600 Arau, Perlis, Malaysia*
[d]*Faculty of Integrated Technologies, Universiti Brunei Darussalam, Jalan Tungku Link, Gadong, BE1410, Brunei Darussalam.*
∗Corresponding author. e-mail: salmie@unimap.edu.my

Received 10 May 2026, Revised 25 May 2026, Accepted 5 June 2026

ABSTRACT

In intermediate-temperature solid oxide fuel cells (IT-SOFCs), samarium-doped ceria (SDC) is one of the promising electrolytes due to its ability to provide high oxygen-ion conductivity and chemical stability. In this study, SDC electrolyte co-doping with manganese with three concentrations, 1%, 5%, and 10%, was synthesized with a solid-state reaction method and sintered at 1450°C without any calcination process. X-ray diffraction, densification, shrinkage, hardness, and ionic conductivity were done on manganese co-doped SDC electrolyte. X-ray diffraction (XRD) analysis confirmed that all compositions are in tetragonal fluorite structure formation. Co-doping manganese on SDC significantly enhanced the shrinkage from SDC 11.82% to 1Mn-SDC 21.52%. However, this experiment found that shrinkage was not directly correlated with densification; 10Mn-SDC exhibits 16.94% shrinkage and 90.54% relative density, while the optimum composition 1Mn-SDC exhibits 21.52% shrinkage and 90.18% relative density. The optimum composition, 1Mn-SDC, exhibits the highest Vickers hardness of 701.3 HV compared with 402.0 HV for undoped SDC. Impedance spectroscopy shows the conductivity improvement: at 300°C, 1Mn-SDC achieved 9.97×10^{-2} S/cm compared to SDC, which showed a value of 7.1×10^{-4} S/cm. Meanwhile, 800°C 1Mn-SDC reached 25.14 S/cm, outperforming SDC, which achieved 7.28 S/cm. On energy activation, it decreases from 1.27 eV to 0.79 eV, which indicates a lower energy barrier for conduction. These studies demonstrate that co-doping manganese on SDC significantly enhances the mechanical and electrochemical performance of SDC electrolytes, with 1Mn-SDC providing the most balanced combination of hardness and ionic conductivity for IT-SOFC applications.

Keywords: *Intermediate-temperature solid oxide fuel cells, Samarium-doped ceria electrolyte, Co-doping; Ionic conductivity and hardness, Transition element*

1. INTRODUCTION

Since the world is facing the depletion of fossil fuels, which increases the need for alternative and reliable energy technologies. Solid oxide fuel cells (SOFCs) have gained attention due to their high efficiency fuel flexibility and low emissions [1, 2]. Research has shifted towards intermediate-temperature solid oxide fuel cells (IT-SOFCs) that operate at 500 to 800°C that bring advantages such as improved long-term structural stability and reduced operational cost [3–6].

However, reducing temperature often leads to decreased electrochemical performance. During the operation at intermediate temperatures, conventional electrolytes experience significant limitations, including reduced ionic conductivity and incomplete densification, which result in increased porosity, gas leakage, mechanical strength, and overall performance degradation. [7, 8]. Among potential candidates, doped ceria electrolytes are one of the promising materials due to their superior, higher ionic conductivity compared to yttria-stabilized zirconia. Despite its advantages, doped ceria often suffers from grain boundary resistance and limited mechanical integrity [9, 10]. Particularly, samarium-doped ceria (SDC) has gained attention due to its enhanced ionic conductivity arising from oxygen vacancy formation [11, 12]. However, SDC performance is strongly influenced by microstructural features such as grain size and defect interactions, which can limit conductivity [13, 14]. To address these limitations, manganese has been introduced as a co-dopant to SDC due to the ability to modify defect chemistry, enhance diffusion during sintering, and influence grain boundary behavior [15–18]. In general, the introduction of additional dopant can increase oxygen vacancy, lattice expansion, and conductivity [19, 20]. Although manganese can improve densification, ionic transport, and mechanical properties, excessive doping may lead to degradation [21, 22].

Therefore, this study investigates the optimum manganese concentration co-doping on SDC electrolyte synthesized by using the solid-state reaction method. Furthermore, this study investigates the effects of Mn addition on phase stability, densification behavior, shrinkage, mechanical integrity, and ionic conductivity. The research expects that co-doping manganese on SDC enhances overall properties on IT-SOFC applications.

2. METHODOLOGY

Samarium- and manganese-co-doped ceria electrolytes, represented by the chemical formula $Ce_{0.8-x}Mn_xSm_{0.2}O_{2-\delta}$ (x = 0, 0.01, 0.05, and 0.1), were synthesized via the solid-state reaction (SSR) method. Cerium (II) oxide, CeO_2 (99.9% purity, Acros Organics); samarium (III) oxide, Sm_2O_3 (99.95% purity, Sigma-Aldrich); and manganese (IV) oxide, MnO_2 (99% purity, Acros Organics), were employed as starting materials. The materials were weighed in stoichiometric proportions according to the formula as shown in Table 1. After that, the materials were mixed using a mortar and pestle for 1 hour with the addition of ethanol. Moreover, the material is pressed into pellet form by using a manual hydraulic press and cylinder mold with a 15 mm inner diameter under 3000 psi pressure, where the material weighs 3.5 grams. Then, the pellet was sintered at a 1450°C temperature for 5 hours, while the heating and cooling rate was 10 degrees Celsius per minute. In this material preparation, there is no calcination process but only a sintering process after uniaxial die pressing.

X-ray diffraction (XRD) was carried out by crushing sintered samples into fine powder to ensure uniform particle distribution. The powdered samples were placed on a sample holder and levelled to obtain a flat and smooth surface. The XRD patterns were recorded using an X-ray diffractometer with Cu K_α radiation (λ = 1.5406 Å), operated at 40 kV and 30 mA. The data were collected over a scanning range of 2θ = 20° to 80° with a step size of 0.02° and a scanning rate of 2° per minute.

After that, shrinkage measurement was determined through diameter change of the pellet before and after sintering by using a digital vernier caliper with ±0.02 mm accuracy [23]. The shrinkage percentage was calculated as Equation (1):

$$\text{Shrinkage (\%)} = \frac{D_1 - D_2}{D_1} \times 100 \quad (1)$$

where D_1 is the diameter of the sample before sintering and D_2 is the diameter of the sample after the sintering process.

Table 1. Composition of $Ce_{0.8-x}Mn_xSm_{0.2}O_{1.9-\delta}$ (x = 0, 0.01, 0.05, 0.10)

Composition	Sample Abbreviation	Mn mol%
$Ce_{0.8}Sm_{0.2}O_{1.9-\delta}$	SDC	0
$Ce_{0.79}Mn_{0.01}Sm_{0.2}O_{1.9-\delta}$	1Mn-SDC	1.0
$Ce_{0.75}Mn_{0.05}Sm_{0.2}O_{1.9-\delta}$	5Mn-SDC	5.0
$Ce_{0.70}5Mn_{0.1}Sm_{0.2}O_{1.9-\delta}$	10Mn-SDC	10.0

For density measurement, Archimedes' principle has been used to measure pellet density along with distilled water. The theoretical density was derived from the molecular weight and lattice parameter obtained from X-ray diffraction analysis. The relative density was calculated using Equation (2):

$$\text{Relative density} = \frac{\text{Apparent density}}{\text{Theoretical density}} \quad (2)$$

In hardness measurement, the sintered sample underwent rigorous metallographic polishing. The samples were subsequently ground and polished using silicon carbide abrasive paper with 600 to 2000 grit, followed by diamond paste with particle sizes of 10 µm, 5 µm, 1 µm, and 0.1 µm to achieve a smooth and flat finish. Once the pellet was polished, the Vickers hardness test was performed, where the diamond-shape indenter was used by applying a constant load of 1 kg to the pellet surface. The load was maintained for a dwell time of 15 seconds to ensure proper indentation. Then, the length of the diagonal indentation was measured under a microscope, and the Vickers hardness value (HV) was calculated according to the standard formula as shown in Equation (3):

$$HV = 1.891\frac{F}{D^2} \quad (3)$$

where *Hv* is the Vicker hardness value, *F* is the force applied load and *D* is the length of the diagonal impression.

Impedance spectroscopy (IS) was employed to evaluate the ionic conductivity of the sintered samples. To further electrical measurement highly conductive silver paste was applied on both surfaces of the sintered pellet to become the blocking electrode and followed by heat treatment at 700°C for 1 hour to ensure proper contact. The impedance measurement was conducted in the frequency range of 10 Hz to 1 MHz under an air atmosphere and at temperatures ranging from 300°C to 800°C to evaluate the thermally activated process. Though the data achieved in IS, the conductivity was calculated by using Equation (4):

$$\sigma = \frac{L}{RA} \quad (4)$$

where σ is the ionic conductivity of the electrolyte, L is the thickness of the pellet, R is resistance of the pellet and A is the area of the pellet.

3. RESULTS AND DISCUSSION

3.1. Phase & Structural Analysis

Figure 1 presents the X-ray diffraction patterns of SDC and Mn-doped SDC electrolytes sintered at 1450°C between the 2θ range of 20°–80°. All samples exhibit diffraction peaks characteristic of a tetragonally distorted fluorite structure, with the major reflections observed at approximately 28.56°, 33.08°, 47.46°, 56.29°, and 59.02°, corresponding to the (110), (200), (220), (310), and (320) planes, respectively, according to ICDD reference code No. 00-038-

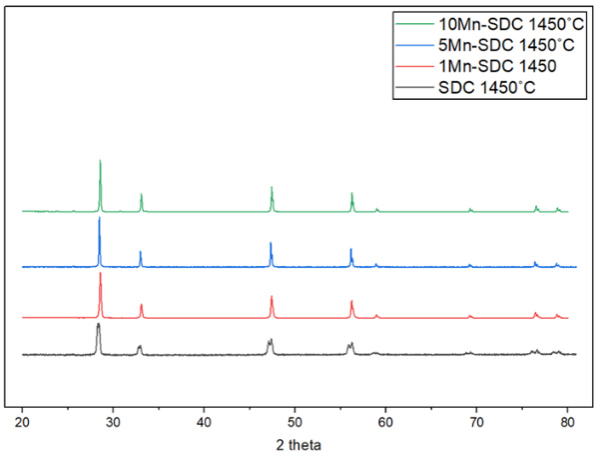

Figure 1. X-ray diffraction patterns of undoped SDC and Mn-doped SDC electrolytes sintered at 1450°C

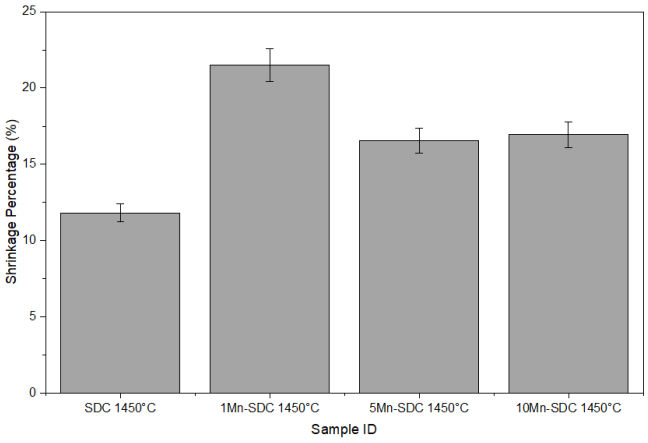

Figure 2. Shrinkage percentage of SDC and Mn-SDC electrolytes sintered at 1450°C

1436 [24]. It can be noticed that Mn doped samples show relatively sharper diffraction peaks compared to SDC, suggesting the role of Mn as sintering aid that improved the crystallinity and well-developed crystal growth [25]. Although the diffraction patterns are consistent with ceria lattice but there is peak splitting occur at 2θ ≈ 33°, 47°, 56° and 76° for SDC. While 2θ ≈ 47°, 56° and 76° for Mn-SDC samples. These observations indicate that the samples are under tetragonal structure.

Table 2 shows lattice parameter and unit cell volume for the samples sintered at 1450°C. All samples show tetragonal structure, since all the lattice parameter $a = b \neq c$. lattice parameters were calculated under tetragonal approximation for distorted fluorite structure. The main diffraction peak for SDC is located at 28.45°, while 1Mn-SDC, 5Mn-SDC and 10Mn-SDC are located at 28.55°, 28.50° and 28.53° respectively. According to Bragg's law, an increase in diffraction angle corresponds to a reduction in interplanar spacing, indicating a minor contraction of the crystal lattice [26, 27]. This behavior suggests that Mn ions are substituted into the ceria lattice, leading to subtle structural adjustments. Although the XRD result shows undoped SDC and Mn co-doped SDC is under tetragonal structure, but Mn helps reduce peak broadening compared to undoped SDC [28].

Table 2. Lattice parameter and unit cell volume of SDC and Mn-doped SDC electrolytes

Sample ID	a (Å)	b (Å)	c (Å)
SDC 1450°C	3.730	3.730	5.320
1Mn-SDC°C	3.721	3.721	5.300
5Mn-SDC°C	3.720	3.720	5.310
10Mn-SDC°C	3.718	3.718	5.290

3.2. Shrinkage Analysis

Figure 2 shows the shrinkage of the samples sintered at 1450°C with various manganese concentration. The undoped SDC sample exhibits shrinkage value of 11.82%. With the addition of manganese, the shrinkage increases and reaches 21.52% for the 1Mn-SDC sample. As the manganese concentration increased, the shrinkage shows a decreasing trend. The shrinkage percentage drop to 16.57% and 16.94% for 5Mn-SDC and 10Mn-SDC samples, respectively. Although the samples are higher than the undoped SDC, these values indicate that the extent of shrinkage is reduced compared to the optimum composition. This behavior implies that the effect of manganese on shrinkage is most significant at lower concentrations, while higher additions lead to microstructural degradation and grain boundary saturation, which hinders further mass transport [29]. Overall, shrinkage results at 1450°C show that small amount of manganese produces the greatest increase in shrinkage, with 1Mn-SDC sample showing the highest value among all compositions.

3.3. Densification

Figure 3 shows the relative density and shrinkage behavior of SDC and Mn-doped SDC electrolytes sintered at 1450°C. The relative density increases from 86.89% for undoped SDC, while 90.18%, 987.54% and 90.54% for 1Mn-SDC, 5Mn-SDC and 10Mn-SDC respectively. This trend indicates that by doping Mn into SDC promote sintering process and facilitate pore elimination during densification.

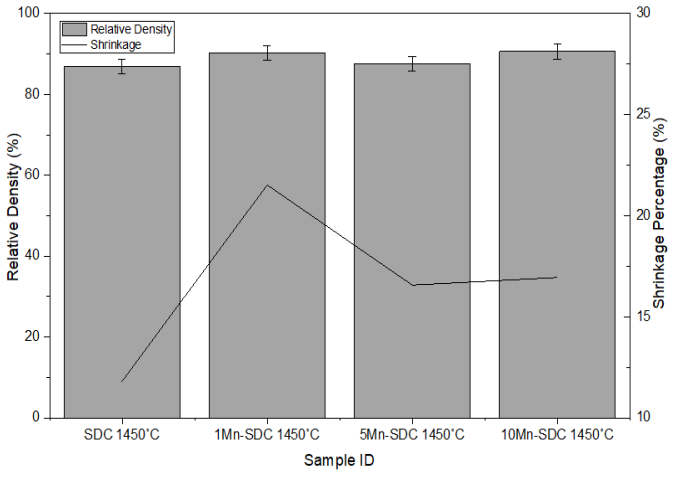

Figure 3. Relationship between relative density and linear shrinkage of SDC and Mn-SDC sample sintered at 1450°C

While 1Mn-SDC exhibits highest shrinkage of 21.52%, with relative density of 90.18%, 10Mn-SDC achieved comparable densification of 90.54%, despite showing lower shrinkage of 16.94%. In theoretical, density will increase as shrinkage because porosity shrinkage reduces the distance between particles during sintering. However, the factors such as pores and pore coarsening connection will affect the density of the sintered samples behavior [30, 31]. Thus, higher shrinkage value does not always result in higher density, since shrinkage reveals overall dimension reduction while density is affected by pore coarsening and pore elimination during sintering. Overall, this result stated that doping manganese into SDC enhances densification.

3.4. Vicker Hardness

Figure 4 shows the undoped SDC sample exhibits the lowest hardness value, 402.0 HV, among all compositions, indicating its comparatively lower mechanical strength. With the introduction of manganese, the 1Mn-SDC sample hardness reaches 701.3 HV, which reflects improved densification and stronger grain bonding. However, as the manganese content increases further, the hardness declines, where the 5Mn-SDC sample reaches 475.8 HV, followed by the 10Mn-SDC sample at 442.3 HV. This behavior suggests that a small amount of manganese enhances the mechanical properties while excessive doping leads to microstructural defects that compromise structural integrity, resulting in reducing hardness [29]. The variation of indention size corresponds to the changes in mechanical resistance in different manganese concentrations. Figure 5 shows the image of the indenter on various composition pellets, presenting physical impact on the samples. The variation of indentation size corresponds to the changes in mechanical resistance in different manganese concentrations.

3.5. Impedance Spectroscopy

Figure 6 presents the Arrhenius plot for SDC and Mn-SDC electrolytes sintered at 1450°C, where a linear relationship between SigmaT and 1000/T is clearly observed across the temperature range from 300°C to 800°C, indicating a thermally activated ionic hopping mechanism. The undoped SDC sample exhibits the lowest ionic conductivity throughout the temperature range, with a value of 7.1 × 10^{-4} S/cm at 300°C and 7.28 S/cm at 800°C. With manganese incorporation, the ionic conductivity improves significantly, where 1Mn-SDC shows the highest performance with 9.97 × 10^{-2} S/cm at 300°C and 25.14 S/cm at 800°C, demonstrating a substantial enhancement compared to SDC. The 5Mn-SDC sample records 3.84 × 10^{-2} S/cm at 300°C and 12.082 S/cm at 800°C, while the 10Mn-SDC sample exhibits slightly higher conductivity than 5Mn-SDC at 300°C with 7.783 × 10^{-2} S/cm and reaches 13.924 S/cm at 800°C. The calculated activation energy is 1.27 eV for SDC and decreases to 0.79 eV, 0.69 eV, and 0.72 eV for 1Mn-SDC, 5Mn-SDC, and 10Mn-SDC, respectively. This reduction confirms that Mn incorporation enhances oxygen vacancy mobility and reduces the migration barrier, thereby improving the ionic transport properties of the electrolyte.

Overall, the results indicate that manganese doping enhances oxygen ion mobility and improves electrolyte performance at intermediate temperatures while 1Mn-SDC provides the most stable and balanced ionic conductivity among the investigated compositions [17].

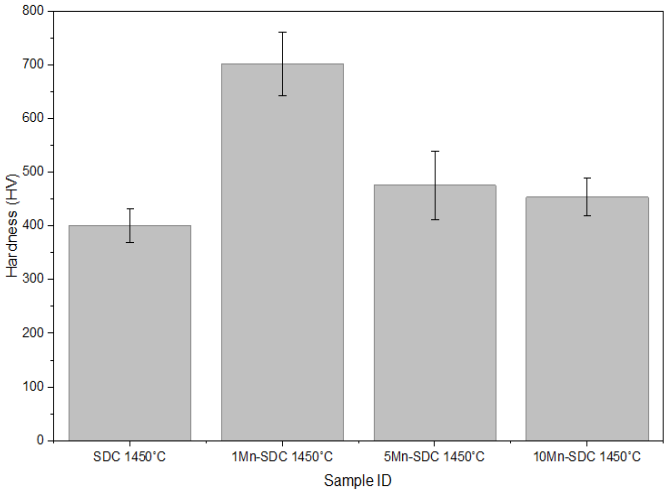

Figure 4. Hardness value of SDC and Mn-SDC electrolytes sintered at 1450°C

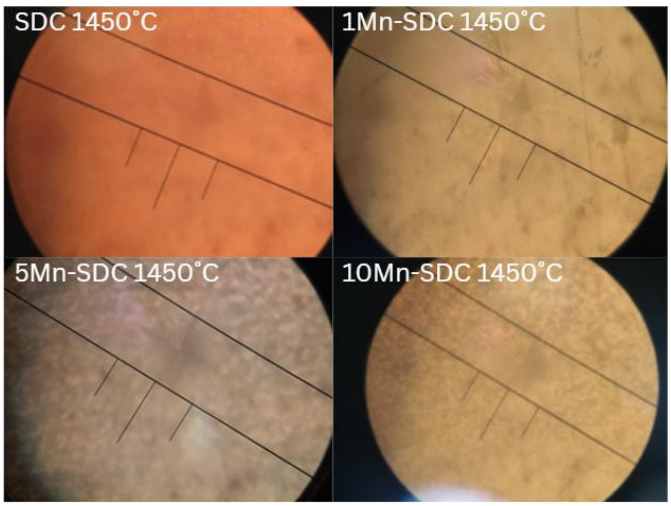

Figure 5. Indenter image under Vickers Hardness experiment

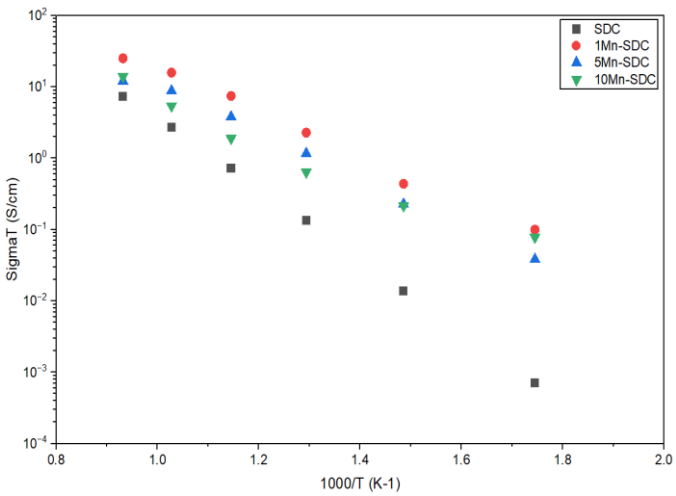

Figure 6. Ionic conductivity of the sample sintered at 1450°C

4. CONCLUSION

The findings of this study demonstrate that manganese co-doping enhances the overall performance of samarium-doped ceria electrolytes sintered at 1450°C. Phase analysis revealed that all compositions stabilized into a tetragonal fluorite structure ($a = b \neq c$).

The addition of manganese significantly improves densification where the relative density increases from 86.89% for undoped SDC to a maximum of 90.54%. However, the results demonstrated that greater shrinkage does not result in higher density. This indicates that densification is controlled not only by dimensional contraction but also by pore elimination efficiency, grain packing, and microstructural development during sintering as well. 10Mn-SDC exhibits the highest relative density (90.54%) despite not showing the greatest shrinkage (16.94%).

After that, the optimum is 1Mn-SDC electrolyte, which produces the highest Vickers hardness (701.3 Hv) and ionic conductivity (25.14 S/cm) at 800°C. This 1Mn-SDC shows a balance improvement between mechanical strength and electrical performance. The objective of finding the optimum concentration is an effective strategy for enhancing the overall properties of SDC electrolytes and highlights the potential of Mn-SDC as a promising electrolyte material for intermediate-temperature solid oxide fuel cell applications.

ACKNOWLEDGMENTS

The author would like to acknowledge the support from the Postgraduate Grant Universiti Malaysia Perlis 2025 (9001-00807) and Fundamental Research Grant Scheme (FRGS) under a grant number of FRGS/1/2020/STG05/UNIMAP/02/4 from the ministry of Higher Education (MoHE) Malaysia.

REFERENCES

[1] D. Radhika and A. S. Nesaraj, "Materials and Components for Low Temperature Solid Oxide Fuel Cells – an Overview," *International Journal of Renewable Energy Development*, vol. 2, no. 2, pp. 87–95, 2013, doi: 10.14710/ijred.2.2.87-95.

[2] B. Rijo, C. Mateos-Pedrero, J. R. Copa Rey, A. Longo, P. Brito, and C. Nobre, "A review of solid oxide cell technologies for power, fuel, and reversible energy storage," *Fuel*, vol. 408, p. 137624, 2026, doi: 10.1016/j.fuel.2025.137624.

[3] C. Sun, "Advances in nanoengineering of cathodes for next-generation solid oxide fuel cells," *Inorganic Chemistry Frontiers*, vol. 11, no. 23, pp. 8164–8182, 2024, doi: 10.1039/D4QI02451F.

[4] A. F. Mohd Abd Fatah, A. Z. Rosli, A. A. Mohamad, A. Muchtar, T. U. Noh, and N. A. Hamid, "Structural characterization and performance optimization of LSCF–based mechanical physical composite cathodes for intermediate–temperature solid oxide fuel cells: A review," *Materials Today Communications*, vol. 41, p. 110597, 2024, doi: 10.1016/j.mtcomm.2024.110597.

[5] H. Shi, C. Su, R. Ran, J. Cao, and Z. Shao, "Electrolyte materials for intermediate-temperature solid oxide fuel cells," *Progress in Natural Science: Materials International*, vol. 30, no. 6, pp. 764–774, 2020, doi: 10.1016/j.pnsc.2020.09.003.

[6] M. Shahid, "Recent advances in protonconducting electrolytes for solid oxide fuel cells," *Ionics*, vol. 28, no. 8, pp. 3583–3601, 2022, doi: 10.1007/s11581-022-04629-w.

[7] A. O. Zhigachev, V. v. Rodaev, D. v. Zhigacheva, N. v. Lyskov, and M. A. Shchukina, "Doping of scandia-stabilized zirconia electrolytes for intermediate-temperature solid oxide fuel cell: A review," *Ceramics International*, vol. 47, no. 23, pp. 32490–32504, 2021, doi: 10.1016/j.ceramint.2021.08.285.

[8] Z. Zakaria, S. H. Abu Hassan, N. Shaari, A. Z. Yahaya, and Y. Boon Kar, "A review on recent status and challenges of yttria stabilized zirconia modification to lowering the temperature of solid oxide fuel cells operation," *International Journal of Energy Research*, vol. 44, no. 2, pp. 631–650, 2020, doi: 10.1002/er.4944.

[9] T. H. S. Silva *et al.*, "Effects of gadolinia doping on densification and electrical properties of $Ce_{0.99-x}Gd_xCu_{0.01}O_{2-\delta}$ solid solutions," *Cerâmica*, vol. 63, no. 368, pp. 470–477, 2017, doi: 10.1590/0366-69132017633682141.

[10] G. Accardo, C. Ferone, and R. Cioffi, "Influence of Lithium on the Sintering Behavior and Electrical Properties of $Ce_{0.8}Gd_{0.2}O_{1.9}$ for Intermediate-Temperature Solid Oxide Fuel Cells," *Energy Technology*, vol. 4, no. 3, pp. 409–416, 2016, doi: 10.1002/ente.201500275.

[11] A. Solovyev, A. Shipilova, and E. Smolyanskiy, "Solid Oxide Fuel Cells with Magnetron Sputtered Single-Layer SDC and Multilayer SDC/YSZ/SDC Electrolytes," *Membranes*, vol. 13, no. 6, p. 585, 2023, doi: 10.3390/membranes13060585.

[12] D. R. Pal and K. Mohan Kant, "Comprehensive Analysis of $Ce_{1-x}Sm_xO_{2-\delta}$ Solid Electrolytes: Structural, Microstructural, and Electrochemical Characterization for Intermediate Temperature Solid Oxide Fuel Cells," *ECS Journal of Solid State Science and Technology*, vol. 12, no. 8, p. 083012, 2023, doi: 10.1149/2162-8777/acec9d.

[13] P. Arunkumar, P. Panda, M. Sribalaji, R. Ramaseshan, A. K. Keshri, and K. S. Babu, "Enhancing the oxygen ionic conductivity of (111) oriented $Ce_{0.80}Sm_{0.20}O_{2-\delta}$ thin film through strain engineering," *Electrochimica Acta*, vol. 240, pp. 437–446, 2017, doi: 10.1016/j.electacta.2017.04.077.

[14] M. R. Kosinski and R. T. Baker, "Preparation and property–performance relationships in samarium-doped ceria nanopowders for solid oxide fuel cell electrolytes," *Journal of Power Sources*, vol. 196, no. 5, pp. 2498–2512, 2011, doi: 10.1016/j.jpowsour.2010.11.041.

[15] T. Zhang, "Effect of transition metal oxides on densification and electrical properties of Si-containing $Ce_{0.8}Gd_{0.2}O_{2-\delta}$ ceramics," *Solid State Ionics*,

vol. 168, no. 1–2, pp. 187–195, 2004, doi: 10.1016/j.ssi.2004.02.015.

[16] S. Farhan, M. Mohsin, A. H. Raza, R. Anwar, B. Ahmad, and R. Raza, "Co-doped cerium oxide $Fe_{0.25-x}Mn_xCe_{0.75}O_{2-\delta}$ as a composite cathode material for IT-SOFC," *Journal of Alloys and Compounds*, vol. 906, p. 164319, 2022, doi: 10.1016/j.jallcom.2022.164319.

[17] S. Li *et al.*, "Oxidative reactivity enhancement for soot combustion catalysts by co-doping silver and manganese in ceria," *Applied Catalysis A: General*, vol. 570, pp. 299–307, 2019, doi: 10.1016/j.apcata.2018.11.033.

[18] E. Ch. Chee Yu, S. S. Che Abdullah, I. H. Wan Nordin, S. H. M.Salleh, R. A. Malek, and P. Pietrusiewicz, "Enhancing Samarium-Doped Ceria Electrolytes with Manganese for Solid Oxide Fuel Cell," *Archives of Metallurgy and Materials*, pp. 1653–1653, 2025, doi: 10.24425/amm.2025.156245.

[19] L.-M. Xue, S.-B. Li, S.-L. An, N. Li, H.-P. Ma, and M.-X. Li, "Fe-based double perovskite with Zn doping for enhanced electrochemical performance as intermediate-temperature solid oxide fuel cell cathode material," *RSC Advances*, vol. 13, no. 44, pp. 30606–30614, 2023, doi: 10.1039/D3RA04991D.

[20] Md. M. Rahman *et al.*, "Highly Dense $Ba_{0.9}La_{0.1}Ce_{0.7}Zr_{0.1}Y_{0.15}Zn_{0.05}O_{3-\delta}$ Electrolyte Material for Intermediate Temperature Solid Oxide Fuel Cells," *Eurasian Journal of Physics and Functional Materials*, vol. 9, no. 2, pp. 97–103, 2025, doi: 10.69912/2616-8537.1245.

[21] D. Pomykalska, M. M. Bućko, and M. Rękas, "Electrical conductivity of MnO_x–Y_2O_3–ZrO_2 solid solutions," *Solid State Ionics*, vol. 181, no. 1–2, pp. 48–52, 2010, doi: 10.1016/j.ssi.2009.11.018.

[22] G. R. Holcomb and D. E. Alman, "The effect of manganese additions on the reactive evaporation of chromium in Ni–Cr alloys," *Scripta Materialia*, vol. 54, no. 10, pp. 1821–1825, 2006, doi: 10.1016/j.scriptamat.2006.01.026.

[23] K. Singh, S. A. Acharya, and S. S. Bhoga, "Low temperature processing of dense samarium-doped CeO_2 ceramics: sintering and intermediate temperature ionic conductivity," *Ionics*, vol. 13, no. 6, pp. 429–434, 2007, doi: 10.1007/s11581-007-0123-x.

[24] S. Kurajica *et al.*, "Phase composition, morphology, properties and improved catalytic activity of hydrothermally-derived manganese-doped ceria nanoparticles," *Nanotechnology*, vol. 33, no. 13, p. 135709, 2022, doi: 10.1088/1361-6528/ac44ed.

[25] N. Kainbayev *et al.*, "Raman Study of Nanocrystalline-Doped Ceria Oxide Thin Films," *Coatings*, vol. 10, no. 5, p. 432, 2020, doi: 10.3390/coatings10050432.

[26] C. M. R. Remédios *et al.*, "Experimental Evidence for the Influence of Mn^{3+} Concentration on the Impurity Incorporation and Habit Modification Mechanism of Potassium Dihydrogen Phosphate," *Crystal Growth & Design*, vol. 10, no. 3, pp. 1053–1058, 2010, doi: 10.1021/cg8013255.

[27] M. A. Wahab, "Importance of d-Spacing in Diffraction of Crystals," in *Mirror Symmetry: The Mother of all Crystal Symmetries*, M. A. Wahab, Ed., Singapore: Springer Nature Singapore, 2024, pp. 105–142. doi: 10.1007/978-981-99-8361-2_5.

[28] H. Kishimoto *et al.*, "In situ analysis on the electrical conductivity degradation of NiO doped yttria stabilized zirconia electrolyte by micro-Raman spectroscopy," *Electrochimica Acta*, vol. 82, pp. 263–267, 2012, doi: 10.1016/j.electacta.2012.04.148.

[29] D. Wang, Y. Xia, H. Lv, L. Miao, L. Bi, and W. Liu, "$PrBaCo_{2-x}Ta_xO_{5+\delta}$ based composite materials as cathodes for proton-conducting solid oxide fuel cells with high CO_2 resistance," *International Journal of Hydrogen Energy*, vol. 45, no. 55, pp. 31017–31026, 2020, doi: 10.1016/j.ijhydene.2020.08.094.

[30] P. C. Yu, Q. F. Li, J. Y. H. Fuh, T. Li, and L. Lu, "Two-stage sintering of nano-sized yttria stabilized zirconia process by powder injection moulding," *Journal of Materials Processing Technology*, vol. 192–193, pp. 312–318, 2007, doi: 10.1016/j.jmatprotec.2007.04.097.

[31] D. Panthi, N. Hedayat, and Y. Du, "Densification behavior of yttria-stabilized zirconia powders for solid oxide fuel cell electrolytes," *Journal of Advanced Ceramics*, vol. 7, no. 4, pp. 325–335, 2018, doi: 10.1007/s40145-018-0282-4.